Int. J. High Technology Ceramics **4** (1988) 289–299

15

Cyclic Fatigue Testing of Ceramic Materials

T. Soma, M. Masuda, M. Matsui & I. Oda

NGK Insulators Ltd, 2–56 Suda-Cho Mizuho-ku, Nagoya 467, Japan

1 INTRODUCTION

Various high-performance ceramics are currently being studied for use as structural components at high temperatures in heat engines. To design components successfully and utilise these materials, an understanding of the effect of cyclic loading on fatigue failure is required. Few cyclic fatigue data on ceramic materials have been accumulated because testing systems for brittle materials at elevated temperatures have not been well established. This paper describes new ceramic testing systems which have been developed to provide fundamental design data on the fatigue properties of ceramic materials.

The fracture strengths of ceramics are usually evaluated by means of 3- or 4-point bend tests instead of tensile tests. The reason is that, owing to the brittleness of ceramics, the tensile test needs specifically designed jigs and specimens to achieve good alignment, together with special techniques and time for the sample preparation and measurement. The authors previously reported on a tensile testing system, where a cylindrical specimen with button-head ends was used and good alignment could easily be obtained (Soma *et al.*, 1985). In this study, the tensile system has been extended for cyclic fatigue testing at elevated temperatures under various cyclic loading conditions.

Finally, an accelerated cyclic fatigue test system has been developed using a resonant bending method to study the fatigue behaviour in ceramic materials at high endurance.

Int. J. High Technology Ceramics 0267-3762/88/$03·50

2 TENSILE AND COMPRESSIVE TEST

A cylindrical specimen of the button-head type was used for tensile and compressive tests. The gauge diameter and length were typically 6 mm and 20 mm, respectively. The specimen was machined by grinding with diamond tools after firing. The concentricity of the specimen was within 10 μm. The maximum surface roughness was less than 3·2 μm.

Figure 1 shows a schematic view of the tensile and compressive test apparatus. The specimen was fixed by using collet chucks outside the furnace. Spherical bearings were used to align the specimen to the axial direction. The grips were water-cooled. Tensile and compressive loads were hydraulically applied. An infra-red radiant furnace of 12 kW was used. The temperature of the gauge section was maintained uniformly by using platinum mesh, which redistributed the infra-red rays. The temperature variation within the gauge portion was controlled within 5°C up to 1500°C.

The temperature was monitored using three thermocouples attached at the gauge section. The accuracy of the alignment was checked before

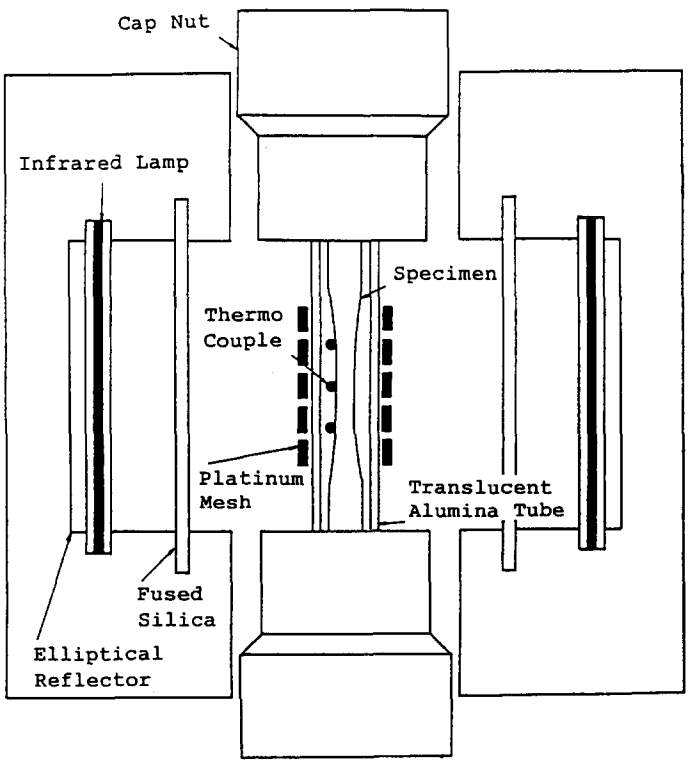

Fig. 1. Schematic diagram of high-temperature cyclic fatigue testing apparatus.

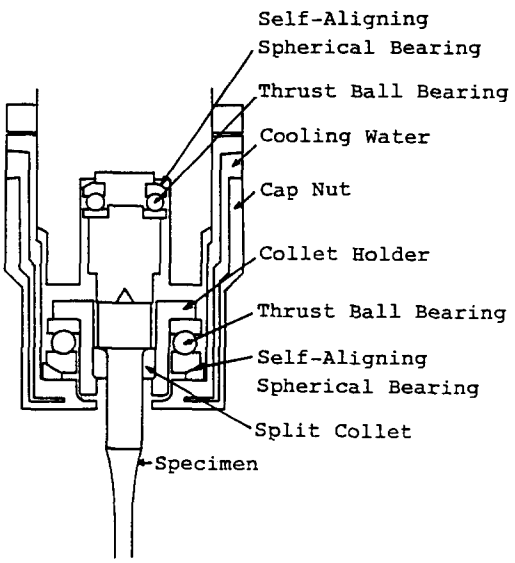

Fig. 2. Gripping arrangement for tension–compression cyclic fatigue test.

heating. The bending stress component was detected using three strain gauges attached at the centre of the gauge section. The alignment was adjusted so that the bending stress component was less than 5%.

Figure 2 shows a schematic view of the grip. A split collet chuck, spherical bearings and thrust ball bearings were used. The spherical surfaces of both upper and lower spherical bearings were concentric. Thrust bearings were

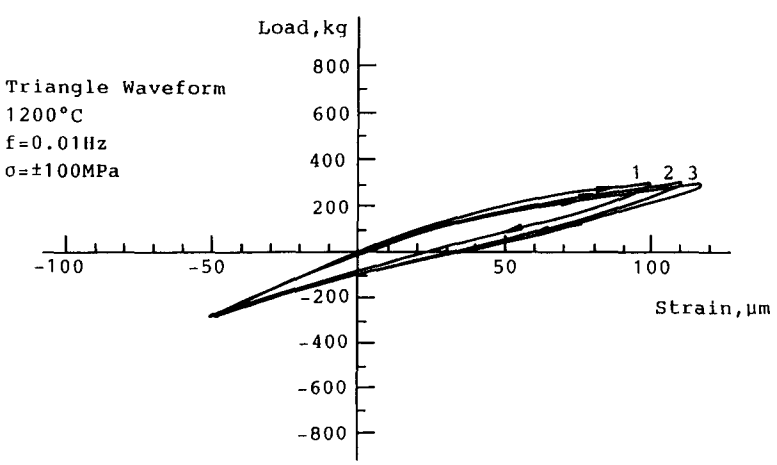

Fig. 3. Stress–strain curve in the cyclic tension–compression test at 1200°C.

used to enable the specimen to rotate easily when adjusting the alignment of the grip and specimen. When assembling the grip, first the compressive load was applied to the button-head of the specimen through the upper spherical bearing and the axis of the alignment was adjusted by monitoring with strain gauges and rotating the specimen. Next, the lower spherical bearing was raised by fastening the cap nut to fix the button-head of the specimen between both spherical bearings.

Figure 3 shows an example of a stress–strain curve for a sintered silicon nitride tested under tension–compression cyclic load at 1200°C. It is

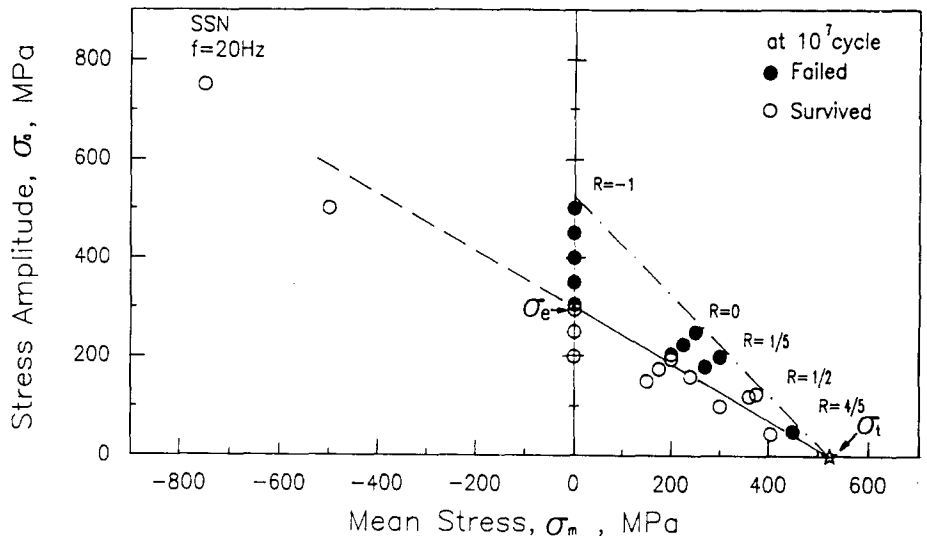

Fig. 4. Stress amplitude versus mean stress for fatigue failure in a sintered silicon nitride at 10^7 cycles in tension–compression and compression–compression tests. The modified Goodman relation is shown by the solid line.

noteworthy that creep strain appears more obviously under tensile load than under compressive load.

Alternating load is often known to accelerate cyclic fatigue in ceramic materials more severely than pulsating load (Soma *et al.*, 1987). The effect of mean stress on the cyclic fatigue behaviour in a sintered silicon nitride was measured by superimposing a steady stress on to the cyclic stress. The frequency was 20 Hz and the ratio, R, of the minimum stress (σ_{min}) to the maximum stress (σ_{max}) was between -1 and $+1$ in tension–tension and tension–compression tests. The measured fatigue data at 10^7 cycles are shown in Figs 4 and 5. The solid line in Fig. 4 shows the modified Goodman

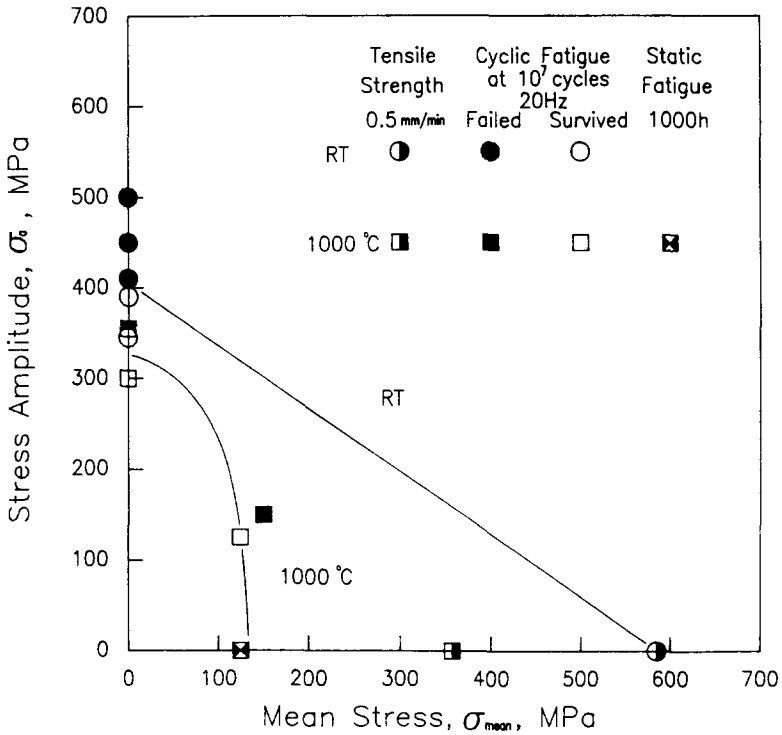

Fig. 5. Cyclic and static fatigue behaviour in a sintered silicon nitride at room temperature and 1000°C.

relation, which is expressed by eqn (1) and is used extensively for designing metallic parts.

$$\sigma_a = \sigma_e\left(1 - \frac{\sigma_m}{\sigma_t}\right) \tag{1}$$

where σ_a is the stress amplitude, σ_m is the mean stress, σ_t is the initial tensile strength and σ_e is the alternating fatigue strength at $R = -1$. It is found that the measured data agree well with the modified Goodman relation. In Fig. 4 it is also shown that ceramic materials exhibit high fatigue resistance to cyclic compression–compression loading at room temperature. In Fig. 5 it is shown that, at high temperature, static fatigue is notable while cyclic fatigue is less damaging.

3 TORSIONAL AND COMBINED STRESS TEST

The specimen for the test under torsional and combined stresses had parallel flats at both ends for applying torsional stress, in addition to tensile and

compressive stresses. Figure 6 shows the disassembled grip and specimen for the torsional and combined stress test. The principal stresses under combined tension–compression–torsion load are given by:

$$\sigma_1 = \frac{\sigma}{2} + \sqrt{\frac{\sigma^2}{4} + \tau^2} \tag{2}$$

$$\sigma_2 = \frac{\sigma}{2} - \sqrt{\frac{\sigma^2}{4} + \tau^2} \tag{3}$$

where σ_1 is the maximum principal stress, σ_2 is the minimum principal stress, σ is the tensile stress due to tensile load and τ is the shear stress due to torsional load. The values of σ and τ are given by:

$$\sigma = \frac{4P}{\pi D^2} \tag{4}$$

$$\tau = \left(\frac{16T}{\pi D^3}\right) \times \left(\frac{2r}{D}\right) \tag{5}$$

where D is the specimen diameter, P is the tensile load, T is the torque and r is the radius variable in the gauge length. The value of τ changes with r and is a maximum at the surface of the specimen. The direction, θ, of the maximum principal stress with respect to the axial direction of the specimen is given by:

$$\theta = \frac{1}{2}\tan^{-1}\left(\frac{2\tau}{\sigma}\right) (0° \leq \theta \leq 90°) \tag{6}$$

Figure 7 shows specimens which have been fractured at room temperature by: pure tension ($\tau = 0$), tension–torsion ($\tau/\sigma = 1$ and 2), pure torsion ($\sigma = 0$) and compression–torsion ($\tau/\sigma = -1$ and -2). The directions of principal stresses are estimated by eqn (6) at $\theta = 0$, 32, 38, 45, 52 and 58°, respectively. Fracture surfaces, which contained fracture origins, were almost perpendicular to the directions of the maximum principal stresses. At elevated temperatures where creep phenomena were significant, θ was found to be smaller than that predicted from eqn (6). This indicates that not only maximum principal stress but also shear stress affects the behaviour in crack propagation at high temperatures.

Figure 8 shows the results of combined stress tests where σ_1 and σ_2 at fracture are plotted as a ratio to the fracture stress in a pure tensile test. σ_1 at fracture increased with increasing positive $\tau:\sigma$ ratios in tension–torsion tests, while it was almost independent of $\tau:\sigma$ for negative $\tau:\sigma$ ratios, coinciding with the value in a pure torsion test. The relation shown by the solid curve in Fig. 8 was derived on the assumption that fracture occurs as a result of the stress perpendicular to the plane of the flaw, taking into account

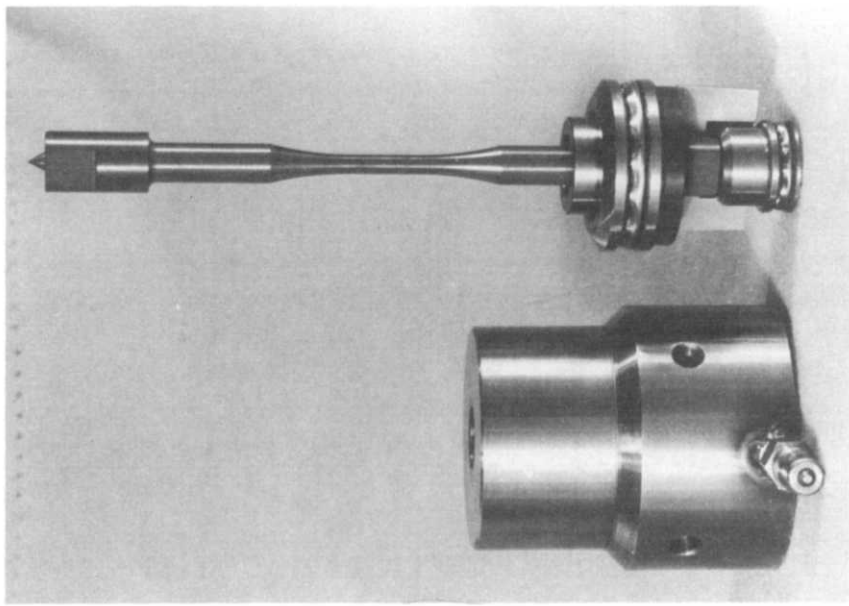

Fig. 7. Typical fractured silicon nitride specimens tested under combined stresses.

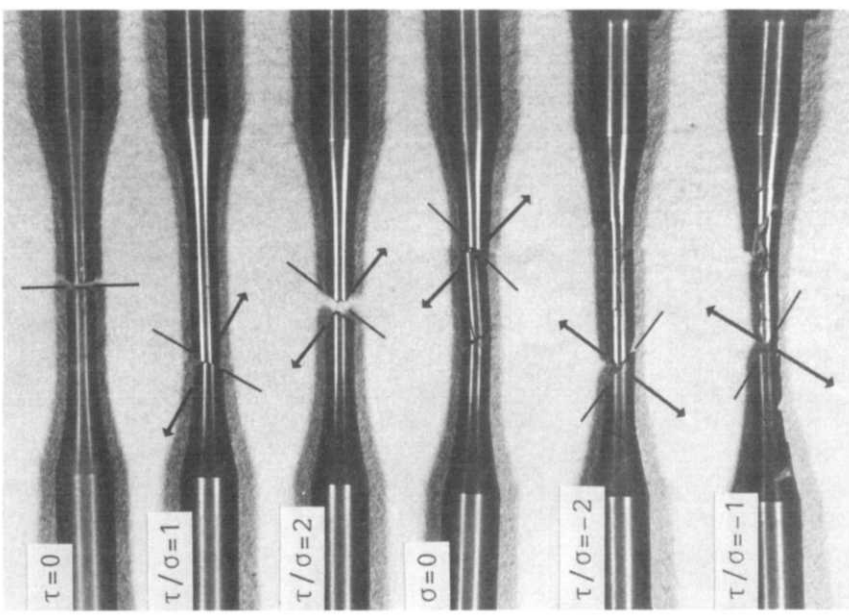

Fig. 6. View of the disassembled grip and specimen for the torsion–tension–compression test.

the size effect on strength according to the Weibull fracture theory. The predicted curve agrees well with test results.

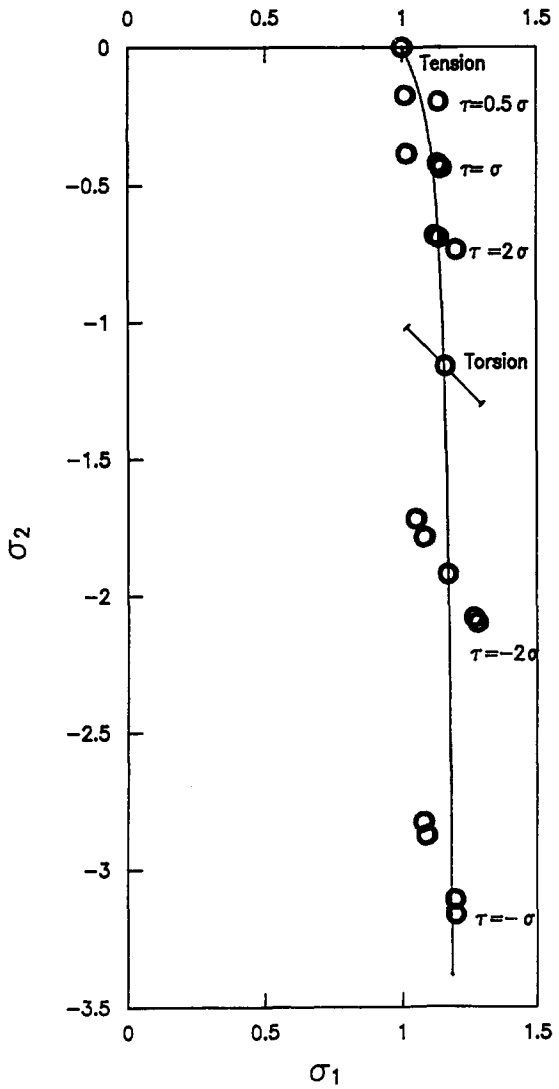

Fig. 8. Plots of fracture stresses in combined tension–torsion tests for a sintered silicon nitride.

4 HIGH-FREQUENCY CYCLIC FATIGUE TEST

Metallic materials, particularly ferritic steels, usually show a fatigue limit at about 10^7 cycles. However in the case of ceramic materials, the number of

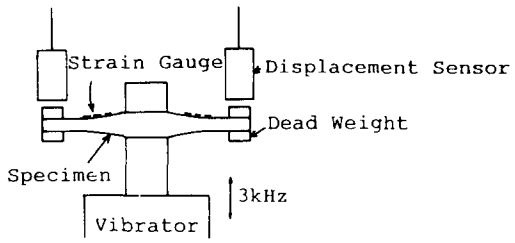

Fig. 9. Schematic diagram of the resonant bending fatigue test.

cycles to failure for several specimens tested exceeded 10^7 cycles, and a fatigue limit did not appear around those cycles. To accumulate fatigue data at up to 10^{10} cycles for ceramic materials, accelerated fatigue tests were carried out by a resonant bending method. No heat was generated in ceramic specimens under cyclic loading at high frequencies, even around 3 kHz, unlike in metals and polymers.

An electro-dynamic vibrator was used in this test at a test frequency of 3 kHz. Figure 9 shows a schematic view of the resonant bending test rig; a tapered beam specimen was used. The weight and the length of the beam was chosen so as to give a resonant frequency of 3 kHz. The maximum tensile stress appeared at the root of the specimen. The cyclic stress amplitude in the tapered beam specimen was measured by strain gauges fixed at the root of

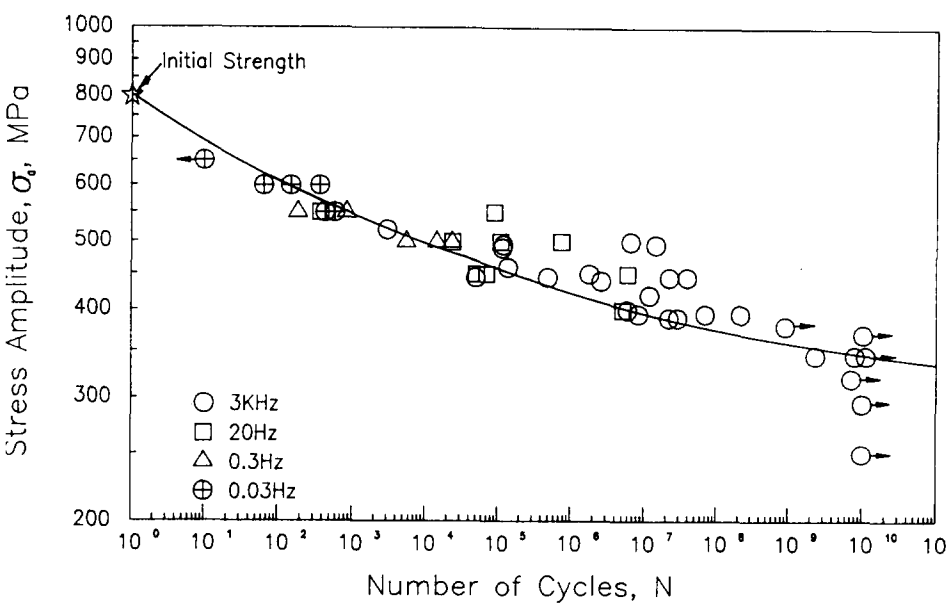

Fig. 10. S–N curve for a sintered silicon nitride.

the specimen. The displacement amplitude of the tip of the specimen was measured by an electro-dynamic sensor whose signal was fed back for controlling the power of the electro-dynamic vibrator to maintain constant cyclic stress. The electro-dynamic sensor was also connected to a cycle counter.

The specimen design used for the resonant bending fatigue test was also used for an alternating cantilever bending fatigue test on a servo-hydraulic test machine. The loading frequency was varied from 0·03 to 20 Hz to study the effect of frequency on the fatigue life of a sintered silicon nitride.

Figure 10 shows the S–N curve derived for the sintered silicon nitride. The solid curve shows the number of cycles to failure, with 50% probability, versus stress amplitude. The shape of this curve suggests the existence of a cyclic fatigue limit. Cyclic fatigue in sintered Si_3N_4 appears to depend principally on the number of cycles rather than on time, because the fatigue strength at various frequencies did not show any systematic variation in the number of the cycles to failure.

5 CONCLUSIONS

(a) A cyclic fatigue testing system using a button-head type cylindrical specimen has been developed. A compact infra-red furnace is used and the specimen is fixed outside the furnace by a self-aligning grip system. Under tension–compression, torsion and combined stresses, cyclic fatigue tests can be successfully conducted up to temperatures of 1500°C.

(b) The effects of mean stress on the cyclic fatigue behaviour of sintered silicon nitride have been measured and a fatigue diagram of the modified Goodman relation obtained.

(c) An accelerated cyclic fatigue testing system has been developed using a resonant bending method. At a frequency of 3 kHz, experiments up to 10^{10} cycles have been successfully conducted at room temperature.

ACKNOWLEDGEMENTS

Part of this work was performed under contract between the Agency of Industrial Science and Technology of MITI and the Engineering Research Association for High Performance Ceramics, as part of the R&D Project: Basic Technology for Future Industries.

REFERENCES

Soma, T., Matsui, M. & Oda, I. (1985). Tensile strength of a sintered silicon nitride. In *Non-Oxide Technical and Engineering Ceramics*, ed. S. Hampshire, Elsevier Applied Science, London, pp. 361–74.

Soma, T., Matsui, M. & Oda, I. (1987). Dynamic fatigue of sintered silicon nitride. In *Proceedings of the International Gas Turbine Congress*, held at Tokyo, Japan, October 1987, I/149–54.